Materials Research Letters

ISSN: (Print) 2166-3831 (Online) Journal homepage: https://www.tandfonline.com/loi/tmrl20

Precipitation kinetics and mechanical properties of nanostructured steels with Mo additions

S. S. Xu, Y. W. Liu, Y. Zhang, J. H. Luan, J. P. Li, L. X. Sun, Z. B. Jiao, Z. W. Zhang & C. T. Liu

To cite this article: S. S. Xu, Y. W. Liu, Y. Zhang, J. H. Luan, J. P. Li, L. X. Sun, Z. B. Jiao, Z. W. Zhang & C. T. Liu (2020) Precipitation kinetics and mechanical properties of nanostructured steels with Mo additions, Materials Research Letters, 8:5, 187-194, DOI: 10.1080/21663831.2020.1734976

To link to this article: https://doi.org/10.1080/21663831.2020.1734976

MATER. RES. LETT.
2020, VOL. 8, NO. 5, 187–194
https://doi.org/10.1080/21663831.2020.1734976

MATERIALS RESEARCH LETTERS
Taylor & Francis
Taylor & Francis Group

ORIGINAL REPORT

Precipitation kinetics and mechanical properties of nanostructured steels with Mo additions

S. S. Xu[a], Y. W. Liu[a], Y. Zhang[a], J. H. Luan[b], J. P. Li[a], L. X. Sun[a], Z. B. Jiao[c], Z. W. Zhang[a,d] and C. T. Liu[b]

[a]Key Laboratory of Superlight Materials and Surface Technology, Ministry of Education, College of Materials Science and Chemical Engineering, Harbin Engineering University, Harbin, People's Republic of China; [b]Department of Materials Science Engineering, College of Science and Engineering, City University of Hong Kong, Hong Kong, People's Republic of China; [c]Department of Mechanical Engineering, The Hong Kong Polytechnic University, Hong Kong, People's Republic of China; [d]Iron & Steel Research Institute of Ansteel Group Corporation, Anshan, People's Republic of China

ABSTRACT

It is known that nanoscale precipitates strongly affect the precipitation hardening of structural materials. In this study, we report the precipitation kinetics and thermostability of Cu-rich and NiAl nanoprecipitates in nanostructured steels with Mo additions. Atom probe tomography and first-principles calculations revealed that the addition of Mo effectively decreased the diffusion coefficients of Cu, Ni and Al atoms, leading to the change in the precipitation mechanisms from NiAl prior-precipitation with an instantaneous-nucleation mechanism to the Cu prior-precipitation with a continuous-nucleation mechanism. The decreased diffusion coefficient significantly improves the thermostability of nanoprecipitates and strongly enhances the strength of the nanostructured steels.

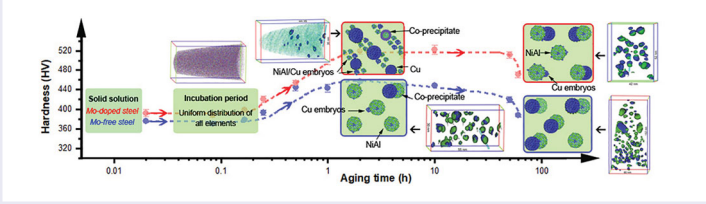

ARTICLE HISTORY
Received 28 December 2019

KEYWORDS
Nanoprecipitates; precipitation mechanisms; thermostability; Mo additions; nanostructured steels

IMPACT STATEMENT

The precipitation mechanisms and thermostability of nanoscale precipitates in nanostructured steels are strongly dependent on the diffusion coefficient of elements, which can be effectively tuned by alloying with Mo additions.

Introduction

Precipitation strengthening has been recognized as one of the most effective methods for strengthening metallic materials [1,2]. Among various particles, Cu and NiAl nanoprecipitates have been widely used in steels for precipitation strengthening [3,4]. The precipitation mechanism and good thermostability for Cu and NiAl nanoprecipitates are vitally important to enable the pursuit of nanoprecipitate-strengthened steels with excellent mechanical properties. The strengthening mechanisms are strongly dependent on the nanoprecipitate properties, including structure, composition, size, number density etc., which are all controlled by the thermostability of these nanoprecipitates [5]. Cu and NiAl nanoprecipitates with a low thermal stability are apt to grow and coarsen during aging, leading to the degradation in the mechanical properties of nanostructured steels [6,7].

Mo, one of the most important alloying elements for steels, is usually added to steels with appropriate amounts for refining grain size, retarding recrystallization, achieving enough hardenability and providing fine carbides [8,9]. Moreover, Mo also has an important effect on the interphase precipitation in nanostructured steels. By reducing the transformation kinetics, Mo increases the

CONTACT Z. W. Zhang zwzhang@hrbeu.edu.cn Key Laboratory of Superlight Materials and Surface Technology, Ministry of Education, College of Materials Science and Chemical Engineering, Harbin Engineering University, Harbin 150001, People's Republic of China; Iron & Steel Research Institute of Ansteel Group Corporation, Anshan, Liaoning 114009, People's Republic of China; C. T. Liu chainliu@cityu.edu.hk Department of Materials Science and Engineering, City University of Hong Kong, Hong Kong, People's Republic of China

Supplemental data for this article can be accessed here. https://doi.org/10.1080/21663831.2020.1734976

volume fraction of interphase precipitates (such as TiC and Ti_2C) in the Ti bearing steels [10]. However, the effects of Mo additions on Cu and NiAl nanoprecipitates have not yet been studied in details. Understanding the effects of Mo on the precipitation mechanisms and thermostability of Cu and NiAl nanoprecipitates is benefit to developing nanostructured steels through simply tuning a common alloying elements Mo to control both the martensite matrix and nanoscale precipitates simultaneously.

In this study, the change in the microstructure and precipitation sequence of Cu and NiAl nanoprecipitates caused by Mo additions were carefully analysed using electron backscattered diffraction (EBSD), transmission electron microscopy (TEM) and atom probe tomography (APT). The effects of Mo on the precipitation sequences of Cu-rich and NiAl-rich nanoprecipitates, their thermostability and mechanical properties are investigated in detail based on the first principle calculations and the experimental results.

Materials and methods

Two nanostructured steels, with compositions of Fe–2.5 Cu–4Ni–1Al–1.5Mn–0.08C–0.5Si (Mo-free) and Fe–2.5 Cu–4Ni–1Al–1.5Mn–0.08C–0.5Si–1.5Mo (wt.%) (Mo-doped), were prepared by arc melting under an argon atmosphere. The ingots were hot rolled at 900°C to a thickness of 2 mm and then solid-solution (SS) treated for 1 h at 900°C, followed by water quenching. The as-quenched samples were then aged separately at 500°C for 5, 10 min (AG10 min), 15, 30 min, 1, 2 h (AG2 h), 5, 10, 50 h (AG50 h) and 60 h. The Vickers hardness measurements were conducted with an applied load of 500 g for 15 s. Ten indents for each specimen were measured to obtain an average value. EBSD and TEM were performed to characterize the phase components and microstructure of the samples. The APT characterizations were performed in a local electrode atom probe (CAMEACA LEAP 5000 R). Imago Visualization and Analysis Software version 3.8 was used for creating the 3D reconstructions and data analyses. Cu- and NiAl-enriched precipitates were identified with the maximum separation method [11]. The 8 at.% Cu concentration and 15 at.% (Ni + Al) concentration isosurfaces are used to visualize the Cu and NiAl nanoprecipitates, respectively. First-principles calculations were implemented with projector-augmented wave potential and the Perdew–Burke–Ernzerh of generalized gradient approximation to describe the Coulomb interaction of ion cores with the valence electrons and the electronic exchange, respectively [12].

Results and discussion

For the Mo-free steel, the hardness has no apparent changes during the first 10 min aging period (Figure 1(a)). After aging for 15 min, the hardness obviously increases and reaches a peak (~456 HV) at 2 h. As for the Mo-doped steel, the hardness under the solid solution condition shows an enhancement of ~20 HV, as compared with that of the Mo-free steel due to the solution strengthening and work hardening caused by Mo additions [13]. Similarly, the hardness of the Mo-doped steel reaches a peak at 2 h. However, the peak value of the hardness (~498 HV) for the Mo-doped steel is obviously higher than that (~456 HV) of the Mo-free steel. Moreover, the peak hardness can sustain from 2 h to 50 h, forming a longstanding harness plateau, indicating that the Mo addition can effectively enhance the age-hardening and the thermostability of the nanoprecipitates.

Many martensite laths with similar average block size (~6.0 μm) were observed both in the Mo-free and Mo-doped steels (Figure 1(b–f)). However, the Mo-doped AG5 h steel has higher dislocation density than the Mo-free AG5 h steel due to the addition of Mo [13]. Weak (100)-type superlattice reflections can be observed in both steels (Figure 1(g)), which have been confirmed to originate from NiAl particles in a similar nanoprecipitation-strengthened steel [14]. This indicates that NiAl nanoprecipitates formed in both steels after aging for 5 h. Mo_2C carbides with a large size, ~50 nm can be observed in the Mo-doped AG50 h steels (Supplementary Figure S1). However, these large Mo_2C carbides with a small number density have no evident effects on the longstanding harness plateau in the Mo-doped steels [15–18].

As for the Mo-free AG10 min sample (Figure 2(a)), all elements are distributed uniformly in the matrix, indicating that no nanoprecipitates exist after aging for 10 min. This is consistent with the micro-hardness results of the Mo-free steel (Figure 1(a)). After aging for 2 h, Cu and NiAl nanoprecipitates are precipitated out (Figure 2(b)). Interestingly, all Cu nanoprecipitates are attached to NiAl nanoprecipitates, forming the Cu/NiAl co-precipitation. However, ~21% (number percent) of individual NiAl nanoprecipitates along with most of the co-precipitates (79%) can be observed in the Mo-free AG2 h steel based on the APT results in Supplementary Figure S2. After aging for 50 h, both the Cu/NiAl co-precipitates and the individual NiAl nanoprecipitates in the Mo-free steel have unevenly coarsened as shown in Figure 2(c) and Table 1. In Figure 2(d,e), Cu, Ni, Al and Mn atoms are obviously enriched in the co-precipitates with the aging time increasing. However, although Ni, Al and Mn atoms

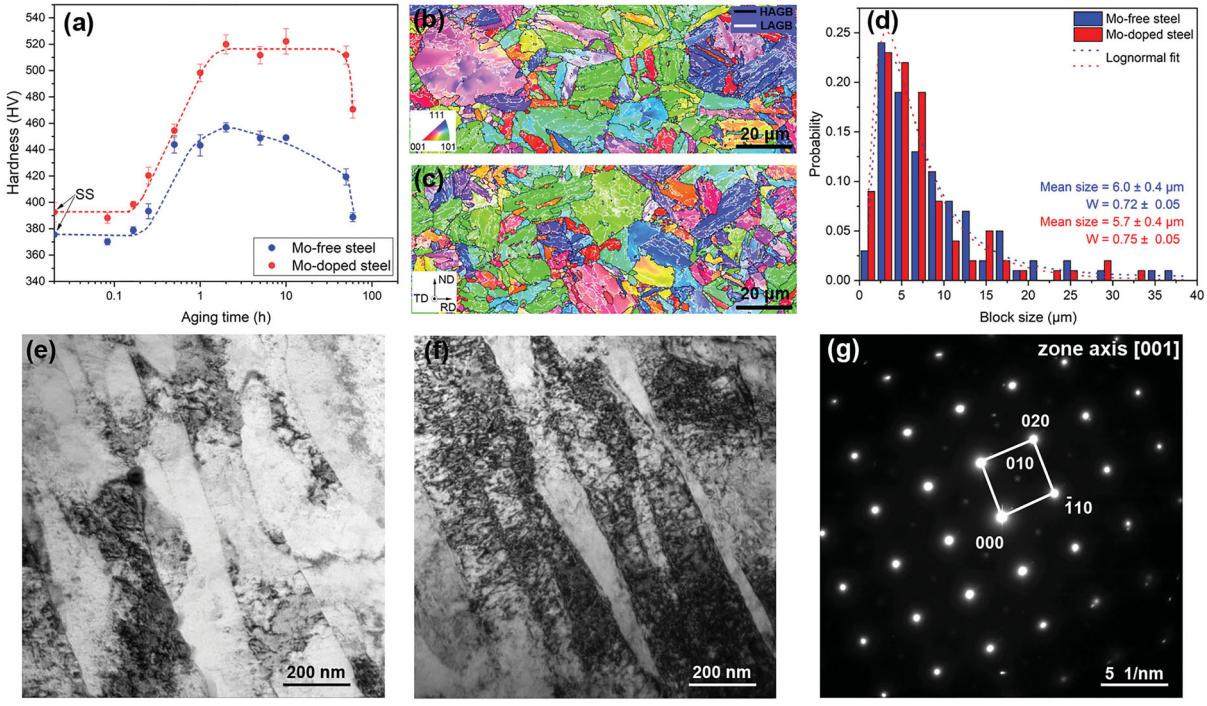

Figure 1. (a) Hardness as a function of aging time for the Mo-free and Mo-doped steel, (b,c) the microstructure and orientation mappings from EBSD for (b) the Mo-free SS and (c) Mo-doped SS steel, and (d) the corresponding grain size distributions. (e,f) TEM bright-field micrographs for (e) the Mo-free and (f) Mo-doped AG5 h steel, and (g) the same respective [001] zone-axis selected area diffraction patterns for two steels with (010)-type superlattice reflections.

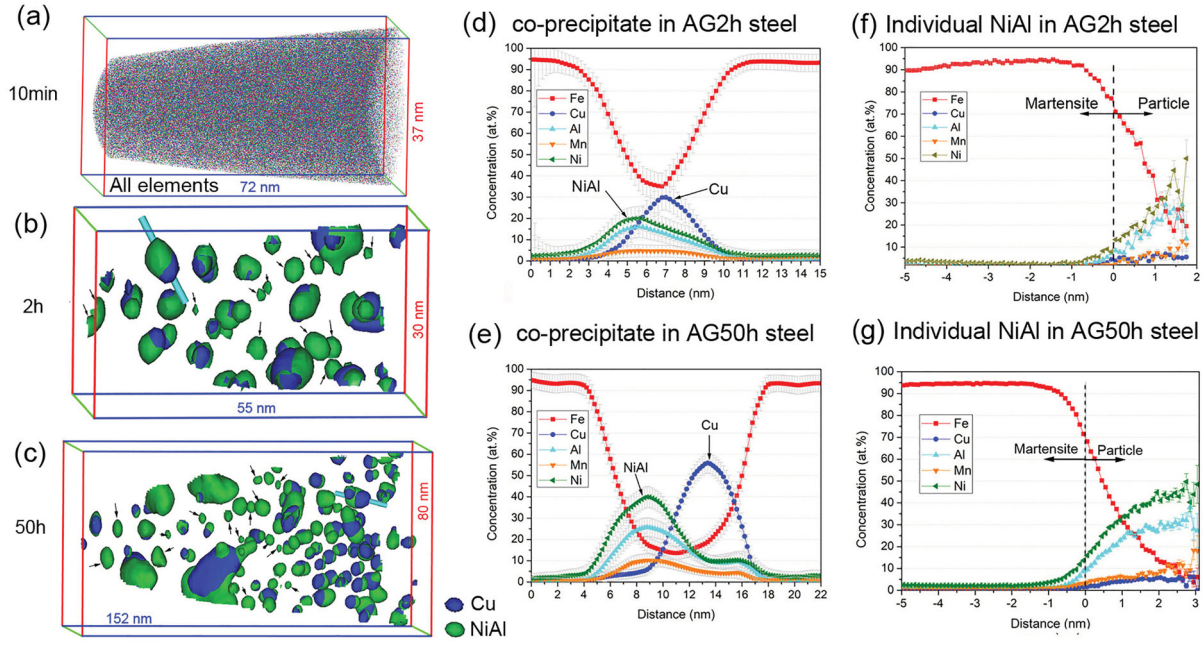

Figure 2. (a) APT atom maps in the Mo-free AG10 min steel, (b,c) APT reconstruction showing size and spatial distribution of co-precipitates and individual NiAl nanoprecipitates (indicated by arrows) in the Mo-free AG2 h (b) and AG50 h steels (c). (d,e) APT atom map along the one-dimensional concentration profiles of a typical co-precipitate (which is indicated by a silver bar in (b,c)) and (f,g) the average proximity histograms of the individual NiAl nanoprecipitates in the Mo-free AG2 h (f) and AG50 h (g) steels.

Table 1. The evolution of nanoprecipitate radius and number density in the Mo-free and Mo-doped steel.

	Aging condition	RadiusCu, nm	Number densityCu, m^{-3}	RadiusNiAl, nm	Number densityNiAl, m^{-3}
Mo-free steel	AG 2 h	1.5 ± 0.5	9.7×10^{23}	1.6 ± 0.5	1.3×10^{24}
	AG 50 h	2.9 ± 1.1	1.5×10^{23}	2.8 ± 0.8	2.6×10^{23}
Mo-doped steel	AG 2 h	1.3 ± 0.5	3.7×10^{23}	0.8 ± 0.2	1.0×10^{23}
	AG 50 h	2.3 ± 0.4	5.9×10^{23}	2.2 ± 0.6	5.8×10^{23}

are also gradually enriched in the individual NiAl nanoprecipitates, but the concentration of Cu remains the value of $\sim 6.2 \pm 2.1$ at.% (Figure 2(f,g)), confirming that Cu precipitates don't separate out from the individual NiAl precipitates. The fraction of individual NiAl nanoprecipitates decreases from $\sim 21\%$ at 2 h to $\sim 16\%$ at 50 h. Therefore, as for the Mo-free steel, NiAl nanoprecipitates firstly nucleate in the matrix after a short incubation period. As the aging time increased, some NiAl precipitates become nucleation sites for Cu atoms to precipitate out from the matrix, forming the Cu/NiAl co-precipitates. Thus, the precipitation sequence in the Mo-free steel can be deduced as 'supersaturated solid solution → incubation period → NiAl → NiAl + Cu', forming a NiAl prior-precipitation mechanism.

As for the Mo-doped steel, an incubation period from SS to 10 min is also observed (see Supplementary Figure S3). After aging for 2 h, some co-segregation regions enriched in Cu, Al and Ni atoms, individual Cu nanoprecipitates and Cu/NiAl co-precipitates are formed in the steel (Figure 3(a)). A high number of Cu and NiAl embryos, which are formed due to local density fluctuations or the nanoscale phase separation in the matrix [19], are responsible for the co-segregation (Supplementary Figure S4). In the Mo-doped AG2 h steel, all the NiAl phase are attached to Cu nanoprecipitates, forming the co-precipitates with the Cu core encased by the NiAl phase. Most of the nanoprecipitates, $\sim 76\%$ are individual Cu-enriched precipitates, which contain small amount of Ni and Al (Figure 3(f)). The nanoprecipitates in the Mo-doped AG2 h steel are quite different from those in the Mo-free AG2 h steel, where the nanoprecipitates consist of $\sim 21\%$ of individual NiAl-enriched nanoprecipitates and 79% of the Cu/NiAl co-precipitates. These results confirmed that the individual Cu nanoprecipitates are firstly separated out, while all NiAl embryos are surrounded by Cu atoms, and finally separated out to form co-precipitates. After aging for 50 h, the co-segregation regions and individual Cu precipitates entirely disappear (Supplementary Figure S5), while a large amount of Cu/NiAl co-precipitates and individual NiAl nanoprecipitates can be identified in

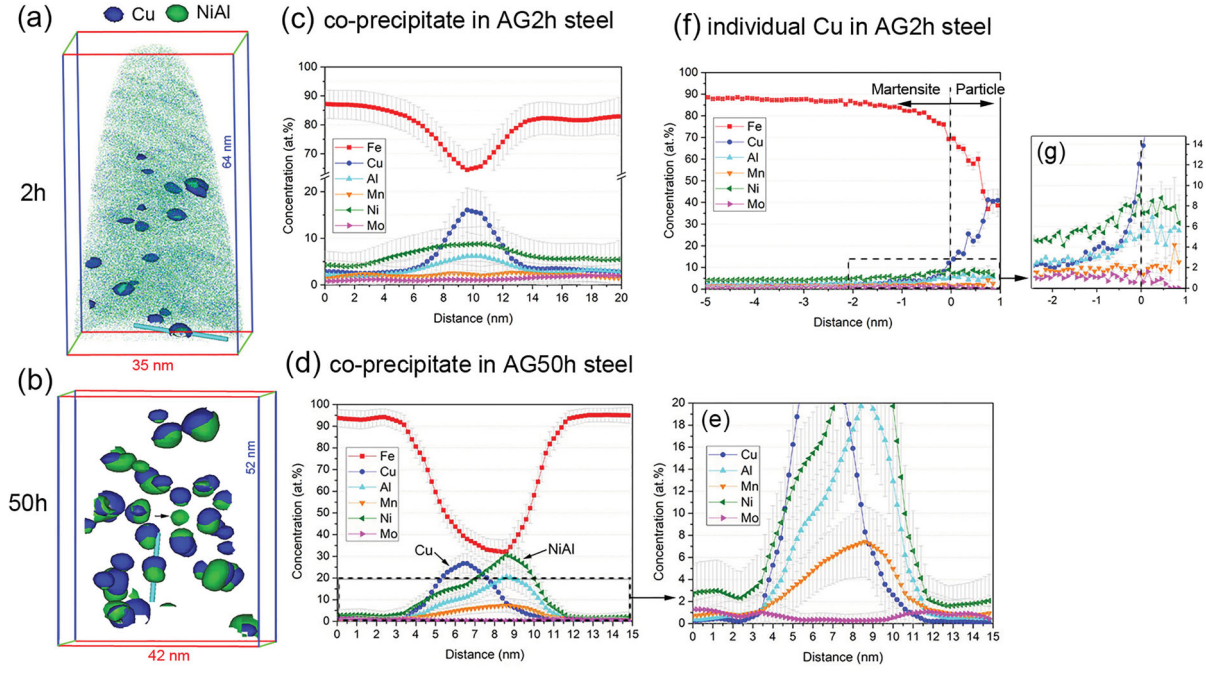

Figure 3. (a,b) APT reconstruction showing size and spatial distribution of nanoprecipitates in the Mo-doped AG2 h (a) and AG50 h (b) steels, and (c,d) the atom maps along with the one-dimensional concentration profiles of the typical co-precipitate in the Mo-doped AG2 h (c) and AG50 h (d) steel with (e) the zoomed-in figures of the doted box in (d), (f) the average proximity histograms of the individual Cu nanoprecipitates in the AG2 h steel with (g) its the zoomed-in figures of the doted box.

Figure 3(b). Therefore, some NiAl embryos can grow out independently, forming the individual NiAl precipitates with the aging time increasing. And most of the individual NiAl precipitates at a late stage can provide nucleation site for Cu precipitates, which is similar to the case in the Mo-free steel, forming the new Cu/NiAl co-precipitates continually and pushing up a high number density of the co-precipitates after aging for 50 h (Figure 3(b)). Moreover, Mo solutes are rejected from all the nanoprecipitates in the Mo-doped AG2 h and AG50 h steel (Figure 3(c–g)).

Therefore, the Mo addition in the nanostructured steels induces the change in the precipitation mechanisms from NiAl prior-precipitation in the Mo-free steel to the Cu prior-precipitation in the Mo-doped steel, as 'supersaturated solid solution → incubation period → Cu → Cu + NiAl' (Figure 4). Moreover, the number density of Cu and NiAl nanoprecipitates in the Mo-free steel is decreased with the growth of the mean radius during the aging treatments, showing a conventional instantaneous-nucleation mechanism [5,20]. However, the mean radius and number density of Cu and NiAl nanoprecipitates both increase in the Mo-doped steel simultaneously (Table 1), indicating that these nanoprecipitates are continuously nucleated upon aging treatments.

Moreover, the coarsening coefficient (k) of Cu and NiAl nanoprecipitates in the two steels are calculated by the Lifshitz, Slyozov and Wagner (LSW) theory [21,22]:

$$R(t)^3 - R(t_0)^3 = kt \quad (1)$$

where $R(t)$ is the average volume-equivalent radius, $R(t_0)$ the initial mean radius, t the aging time and k coarsening coefficient. The results indicate that the coarsening coefficients of Cu and NiAl nanoprecipitates in the Mo-doped steel (0.208 and 0.211 $nm^3\ h^{-1}$, respectively) are much less than that in the Mo-free steel (0.437 and 0.372 $nm^3\ h^{-1}$, respectively). Due to the higher coarsening coefficients in the Mo-free steel, Cu or NiAl nanoprecipitates rapidly gobble up each other to grow, thereby the peak hardness value gradually decreases after aging for 2 h. While the Mo addition slows down this growth process through a decreased coarsening coefficient of nanoprecipitates, forming a peak hardness plateau from aging for 2 to 50 h. Therefore, the Mo addition effectively promotes the thermostability of Cu and NiAl nanoprecipitates in the nanostructured steel.

To investigate the origin of the changes in the precipitation mechanisms and thermostability induced by the addition of Mo, the mixing enthalpies between Mo and Ni/Al/Cu and the effect of Mo on the diffusion rate of Ni, Al and Cu in Fe were evaluated. The mixing enthalpy is −7, −5 and 19 $kJ\,mol^{-1}$ between Mo and Ni/Al/Cu elements, respectively, indicating that Mo tends to attract Ni and Al while repel Cu. To evaluate the diffusion coefficient, the vacancy-mediated diffusion model for a body-centered cubic (BCC) structure developed by nine-frequency model of Le Claire [23] was applied since solute diffusions are generally governed by a monovacancy mechanism on a BCC lattice (Figure 5) [24]. The detailed calculation process is illustrated in supplemental online materials. The diffusion coefficients of Ni, Al and Cu without Mo addition are estimated as 1.93×10^{-21}, 6.08×10^{-20} and $2.29 \times 10^{-20}\ m^2\,s^{-1}$, respectively, which are consistent with the published values with the same order of magnitude [25]. With the Mo addition, the diffusion coefficient for Ni, Al and Cu decrease to 4.80×10^{-23}, 8.72×10^{-22} and $2.35 \times 10^{-22}\ m^2\,s^{-1}$, respectively. It is obvious that Mo indeed decreases the diffusion coefficients of Ni, Al and Cu solutes by almost two orders of magnitude.

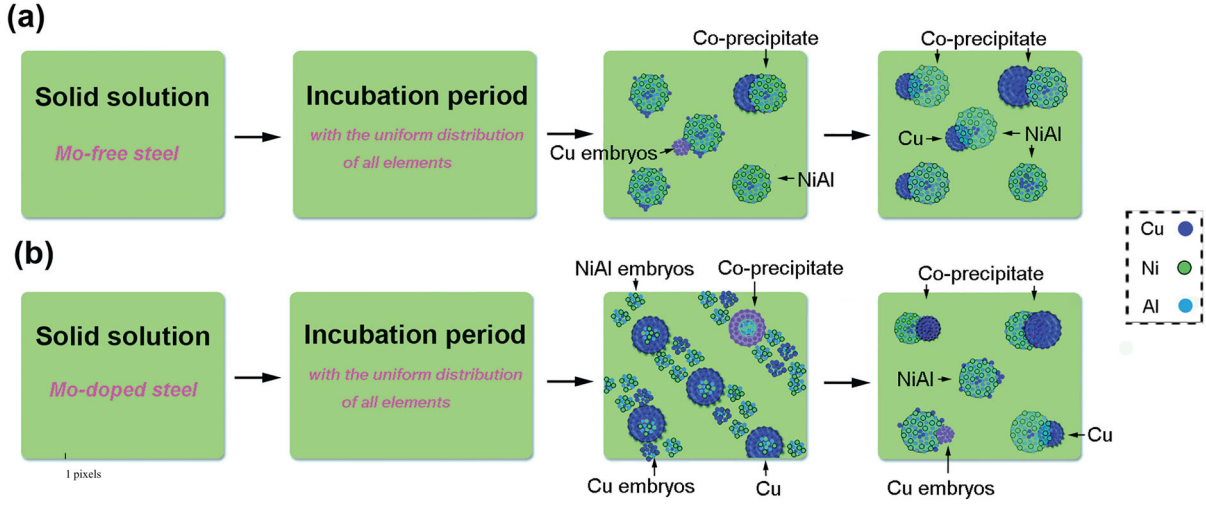

Figure 4. The precipitation mechanism schematics of the NiAl and Cu nanoprecipitates in the Mo-free (a) and Mo-doped (b) steel.

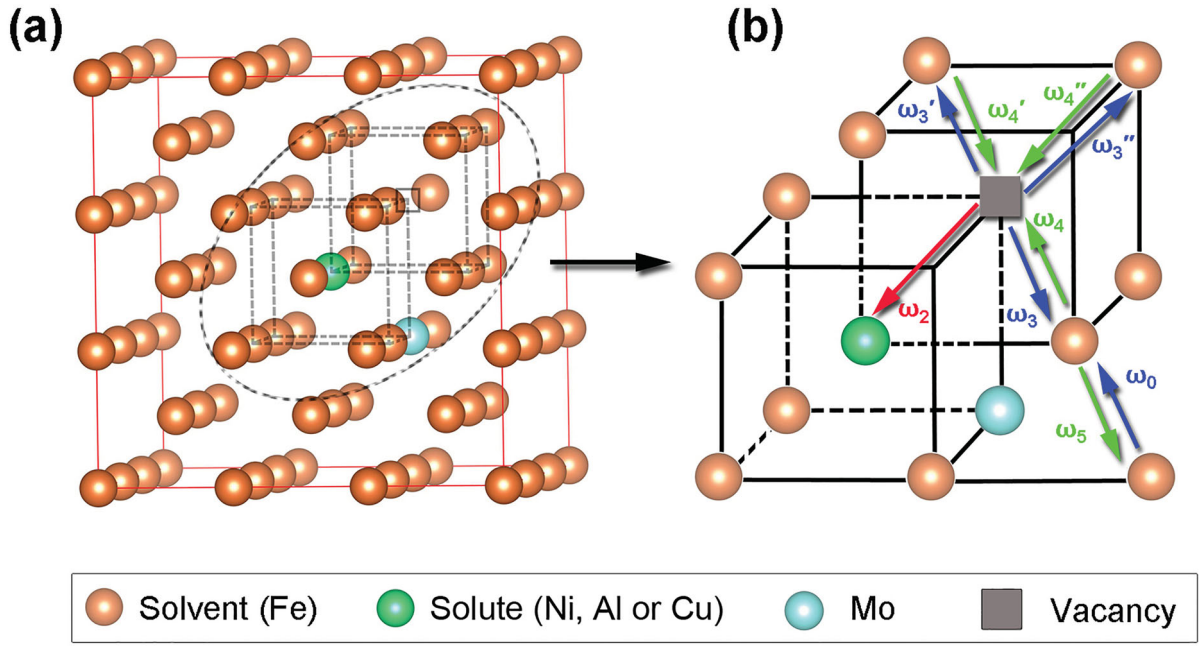

Figure 5. (a) The 54-atoms supercell for first-principles calculations, (b) the schematic illustration of nine-frequency model proposed by Le Claire [23].

It can be seen from the APT and TEM results that there is no segregation or partitioning of Mo in the matrix in Mo-doped AG10min (Supplementary Figure S3), AG2h (Supplementary Figure S4) and AG50h steels (Supplementary Figure S1). Only in AG50h steel were Mo2C carbides observed. This is reasonable since Mo is a heavy element [26], and more aging time was required for diffusion and subsequent partitioning of Mo to Mo_2C carbides [27]. Thus, Mo_2C carbides would nucleate later than Cu and NiAl precipitates, which also observed in the BA-160 [15], HSLA-115 [17] and ultrahigh-strength carburized steels [28]. These indicate that the formation of Cu and NiAl precipitates could not be affected by the Mo partitioning and the formation of Mo2C. Combining the interaction relationship between Mo and Ni/Al/Cu and the decreased diffusion coefficients induced by Mo addition, the scenario of the change in the precipitation mechanisms can be deduced that the interaction relationship between Mo and Ni/Al/Cu atoms influence the nucleation of NiAl and Cu nanoprecipitates while the diffusion coefficient dominates the continuous nucleation and growth of NiAl-enriched and Cu-enriched precipitates. The uniformly distributed Mo atoms in the Mo-doped steel (see Supplementary Figure S3) can impede the formation of NiAl embryos and precipitates due to the negative mixing enthalpies between Mo and Ni/Al, leading to the decrease in the number density of NiAl precipitates in Mo-doped AG2 h steel (1.0×10^{23} m^{-3}), as compared to the Mo-free AG2 h steel (1.3×10^{24} m^{-3}). However, the positive mixing enthalpies between Mo and Cu can promote the precipitation of Cu atoms from the matrix. This can be confirmed by the difference in the number densities of Cu-enriched precipitates in Mo-doped AG2 h steel (3.7×10^{23} m^{-3}) and in Mo-free AG2 h steel (9.7×10^{23} m^{-3}). The reduced diffusion coefficient with the addition of Mo retards the precipitation of both NiAl and Cu nanoprecipitates and promotes their continuous nucleation upon aging, leading to the synergetic increasing of radius and number density of nanoprecipitates. Furthermore, the coarsening rate (k) of Cu and NiAl nanoprecipitates depends on the diffusion coefficient of its constituent elements [29]. Thus, the Mo addition can decrease the coarsening rate of Cu and NiAl nanoprecipitates through deceasing the diffusion coefficients of Ni, Al and Cu solutes, contributing to the good thermostability of NiAl and Cu nanoprecipitates.

Conclusions

The precipitation kinetics and mechanical properties of nanostructured steels with Mo additions have been studied. Uniformly distributed Mo in the Fe matrix can retard the formation of NiAl embryos while promote the formation of Cu embryos due to the attractive effects between Mo and Ni/Al atoms and the repulsive effect between Mo and Cu atoms. The addition of Mo decreased the diffusion coefficients of Cu, Ni and Al atoms. The nucleation and growth of both NiAl and Cu nanoprecipitates were delayed due to the decrease in the diffusion coefficient of

Ni, Al and Cu atoms, thereby inducing transfer of the precipitation mechanisms from a NiAl prior-precipitation with an instantaneous-nucleation mechanism in the Mo-free steel to Cu prior-precipitation sequence with a continuous nucleation mechanism in the Mo-doped steel. Moreover, the decreased diffusion coefficients of Ni, Al and Cu atoms with Mo addition can also contribute to the good thermostability of the precipitates. Adjusting the diffusion coefficient of elements is an effective method to control the nanoscale precipitation and its thermostability.

Disclosure statement

No potential conflict of interest was reported by the author(s).

Funding

This work was supported by the National Key R&D Program of China [2018YFE0115800], NSFHLJ [JC2017012, LH2019E030], Heilongjiang Touyan Innovation Team Program, and China Postdoctoral Science Foundation Funded Project [2019T120255]. Atom probe tomography research was conducted at the Inter-University 3D Atom Probe Tomography Unit of City University of Hong Kong supported by the CityU [grant number 9360161] and CRF [grant number C1027-14E].

References

[1] Sun ZQ, Song G, Ilavsky J, et al. Duplex precipitates and their effects on the room-temperature fracture behaviour of a NiAl-strengthened ferritic alloy. Mater Res Lett. 2015;3:128–134.
[2] Isheim D, Vaynman S, Fine ME, et al. Copper-precipitation hardening in a non-ferromagnetic face-centered cubic austenitic steel. Scripta Mater. 2008;59:1235–1238.
[3] Jiao ZB, Luan JH, Guo W, et al. Atom-probe study of Cu and NiAl nanoscale precipitation and interfacial segregation in a nanoparticle-strengthened steel. Mater Res Lett. 2017;5:562–568.
[4] Kapoor M, Isheim D, Ghosh G, et al. Aging characteristics and mechanical properties of 1600 MPa body-centered cubic Cu and B2-NiAl precipitation-strengthened ferritic steel. Acta Mater. 2014;73:56–74.
[5] Xu SS, Zhao Y, Chen D, et al. Nanoscale precipitation and its influence on strengthening mechanisms in an ultra-high strength low-carbon steel. Int J Plasticity. 2019;113:99–110.
[6] Jiao ZB, Luan JH, Zhang ZW, et al. Synergistic effects of Cu and Ni on nanoscale precipitation and mechanical properties of high-strength steels. Acta Mater. 2013;61:5996–6005.
[7] Kapoor M, Isheim D, Vaynman S, et al. Effects of increased alloying element content on NiAl-type precipitate formation, loading rate sensitivity, and ductility of Cu- and NiAl-precipitation-strengthened ferritic steels. Acta Mater. 2016;104:166–171.
[8] Xia Y, Miyamoto G, Yang ZG, et al. Direct measurement of carbon enrichment in the incomplete bainite transformation in Mo added low carbon steels. Acta Mater. 2015;91:10–18.
[9] Takahashi J, Ishikawa K, Kawakami K, et al. Atomic-scale study on segregation behavior at austenite grain boundaries in boron- and molybdenum-added steels. Acta Mater. 2017;133:41–54.
[10] Gong P, Liu XG, Rijkenberg A, et al. The effect of molybdenum on interphase precipitation and microstructures in microalloyed steels containing titanium and vanadium. Acta Mater. 2018;161:374–387.
[11] Hyde JM, Ellis D, English CA, et al. Microstructural evolution in high nickel submerged arc welds. ASTM Inter. 2001;1405:262–290.
[12] Perdew JP, Burke K, Ernzerhof M. Generalized gradient approximation made simple. Phys Rev Lett. 1996;77:3865–3868.
[13] De Luca A, Seidman DN, Dunand DC. Effects of Mo and Mn microadditions on strengthening and over-aging resistance of nanoprecipitation-strengthened Al-Zr-Sc-Er-Si alloys. Acta Mater. 2019;165:1–14.
[14] Wen YR, Hirata A, Zhang ZW, et al. Microstructure characterization of Cu-rich nanoprecipitates in a Fe-2.5 Cu-1.5 Mn-4.0 Ni-1.0 Al multicomponent ferritic alloy. Acta Mater. 2013;61:2133–2147.
[15] Mulholland MD, Seidman DN. Nanoscale co-precipitation and mechanical properties of a high-strength low-carbon steel. Acta Mater. 2011;59:1881–1897.
[16] Jain D, Isheim D, Seidman DN. Carbon redistribution and carbide precipitation in a high-strength low-carbon HSLA-115 steel studied on a nanoscale by atom probe tomography. Metall Mater Trans A. 2017;48:3205–3219.
[17] Jain D, Isheim D, Hunter AH, et al. Multicomponent high-strength low-alloy steel precipitation-strengthened by sub-nanometric Cu precipitates and M_2C carbides. Metall Mater Trans A. 2016;47:3860–3872.
[18] Huang D, Yan J, Zuo X. Co-precipitation kinetics, microstructural evolution and interfacial segregation in multicomponent nano-precipitated steels. Mater Charact. 2019;155:109786.
[19] Zhang ZW, Liu CT, Wang XL, et al. From embryos to precipitates: a study of nucleation and growth in a multicomponent ferritic steel. Phys Rev B. 2011;84:174114.
[20] Wen YR, Li YP, Hirata A, et al. Synergistic alloying effect on microstructural evolution and mechanical properties of Cu precipitation-strengthened ferritic alloys. Acta Mater. 2013;61:7726–7740.
[21] Wagner CZ, Elektrochem Z. Theory of precipitate change by redissolution. Angew Phys Chem. 1961;65:581–591.
[22] Lifshitz IM, Slyozov VV. The kinetics of precipitation from supersaturated solid solutions. J Phys Chem Solids. 1961;19:35–50.
[23] Le Claire AD. Solvent self-diffusion in dilute b.c.c. solid solutions. The Philos Mag. 1970;21:819–832.
[24] Huang SY, Worthington DL, Asta M, et al. Calculation of impurity diffusivities in alpha-Fe using first-principles methods. Acta Mater. 2010;58:1982–1993.
[25] Versteylen CD, van Dijk NH, Sluiter MHF. First-principles analysis of solute diffusion in dilute bcc Fe-X alloys. Phys Rev B. 2017;96:094105.

[26] Gale WF, Totemeier TC. Smithells metals reference book. 8th ed. Amsterdam: Elsevier; 2004.
[27] Moon J, Park SJ, Jang JH, et al. Atomistic investigations of κ-carbide precipitation in austenitic Fe-Mn-Al-C lightweight steels and the effect of Mo addition. Scripta Mater. 2017;127:97–101.
[28] Tiemens BL, Sachdev AK, Olson GB. Cu-precipitation strengthening in ultrahigh-strength carburizing steels. Metall Mater Trans A. 2012;43:3615–3625.
[29] Umantsev A, Olson GB. Ostwald ripening in multicomponent alloys. Scripta Metall. 1993;29:1135–1140.